Article Type: Research Article

Validation and application of a fast Monte Carlo algorithm for assessing the clinical impact of approximations in analytical dose calculations for pencil beam scanning proton therapy

Sheng Huang[1,2*], Kevin Souris[3], Siyang Li[1], Minglei Kang[1], Ana Maria Barragan Montero[3], Guillaume Janssens[4], Alexander Lin[1], Elizabeth Garver[1], Christopher Ainsley[1], Paige Taylor[5], Ying Xiao[1], Liyong Lin[1,6]

[1]Department of Radiation Oncology, University of Pennsylvania, 3400 Civic Central Blvd, Philadelphia, PA19104, USA

[2]Department of Medical Physics, Memorial Sloan Kettering Cancer Center, 1275 York Ave, New York, NY10065, USA

[3]Center for Molecular Imaging and Experimental Radiotherapy, Institut de Recherche Expérimentale

et Clinique, Université catholique de Louvain, Avenue Hippocrate 54, 1200 Brussels, Belgium

and ICTEAM Institute, Université catholique de Louvain, Louvain-la-Neuve 1348, Belgium

[4]Advanced Technology Group, Ion Beam Applications SA, Louvain-la-Neuve, Belgium

[5]The Imaging and Radiation Oncology Core Houston Quality Assurance Center, The University of Texas

MD Anderson Cancer Center, 8060 EL RIO St Houston, TX 77054, USA

[6]Department of Radiation Oncology, Winship Cancer Institute at Emory University, 1365 Clifton Rd. Atlanta, GA 30322, USA

Corresponding author: Sheng Huang, Ph.D.

Mailing address: 1275 York Avenue, Box 84, New York, NY 10065

Email: huasonwang@gmail.com

This article has been accepted for publication and undergone full peer review but has not been through the copyediting, typesetting, pagination and proofreading process, which may lead to differences between this version and the Version of Record. Please cite this article as doi: 10.1002/mp.13231

Abstract

Purpose: Monte Carlo (MC) dose calculation is generally superior to analytical dose calculation (ADC) used in commercial TPS to model the dose distribution especially for heterogeneous sites, such as lung and head/neck patients. The purpose of this study is to provide a validated, fast and open-source MC code, MCsquare, to assess the impact of approximations in ADC on clinical pencil beam scanning (PBS) plans covering various sites.

Methods: First, MCsquare was validated using tissue-mimicking IROC lung phantom measurements as well as benchmarked with the general-purpose Monte Carlo TOPAS for patient dose calculation. Then a comparative analysis between MCsquare and ADC were performed for a total of 50 patients with 10 patients per site (including liver, pelvis, brain, head-and-neck and lung). Differences among TOPAS, MCsquare and ADC were evaluated using four dosimetric indices based on the dose-volume histogram (target Dmean, D95, homogeneity index, V95), a 3D gamma-index analysis (using 3 %/3 mm criteria), and estimations of tumor control probability (TCP).

Results: Comparison between MCsquare and TOPAS showed less than 1.8 % difference for all of the dosimetric indices/TCP values and resulted in a 3D gamma index passing rate for voxels within the target in excess of 99 %. When comparing ADC and MCsquare, the variances of all the indices were found to increase as the degree of tissue heterogeneity increased. In the case of lung, the D95s for ADC were found to differ by as much as 6.5 % from the corresponding MCsquare statistic. The median gamma index passing rate for voxels within the target volume decreased from 99.3 % for liver to 75.8 % for lung. Resulting TCP differences can be large for lung (≤ 10.5 %) and head-and-neck (≤ 6.2 %), while smaller for brain, pelvis and liver (≤ 1.5 %).

Conclusions: Given the differences found in the analysis, accurate dose calculation algorithms such as Monte Carlo simulations are needed for proton therapy, especially for disease sites with high heterogeneity, such as head-and-neck and lung. The establishment of MCsquare can facilitate patient plan reviews at any institution and can potentially provide unbiased comparison in clinical trials given its accuracy, speed and open source availability.

Key Words: pencil beam scanning, proton therapy, Monte Carlo, fast Monte Carlo

1. Introduction

Dose calculation accuracy is essential to achieve optimal treatment plans for proton radiation therapy and to fully exploit its advantages over traditional photon therapy. Analytical dose calculations (ADCs) are typically used in commercial treatment planning systems (TPSs) for clinical practice because they can provide reasonable accuracy with high computational speed[1-7]. In ADC, proton fluence is predicted by using the water-equivalent thickness along the central path of a pencil beam and by assuming that the medium is laterally homogeneous. However, these simplifications lead to inaccurate modeling of the Multiple Coulomb scattering (MCS) process and thus cause both dose distortion and range uncertainties, especially when protons propagate through bone-soft tissue, soft tissue-air, or bone-air interfaces in treatment sites such as brain, lung, and head/neck[8-10]. Furthermore, approximations in the modeling of elastic and inelastic nuclear interactions in ADC can also cause inaccurate dose distributions even in a homogeneous medium[11,12].

To assess the dose inaccuracy issues in ADC, Monte Carlo (MC) dose calculations such as Geant4[13], MCNPX[14], FLUKA[15], and extension toolkits like TOPAS[16] and GATE[17], based on Geant4[9,10,18-21], have been widely used. However, the routine use of these general purpose MC codes in the clinic for post-planning dose verification or treatment planning is significantly hindered by their long computation time and their lack of availability in community hospitals. Therefore, various fast MC codes have been developed for proton therapy using different strategies in order to accelerate the computation speed while preserving the accuracy of a general purpose MC code. For instance, simplification of the physical models and optimization of the algorithmic implementation can substantially reduce the calculation time[22,23]. Fippel and Soukup[11] introduced a simplified MC algorithm for voxelized geometries which had been previously applied to photons and electrons[24], and Li et al[25] developed a track-repeating algorithm based on pre-computed trajectories and interactions for various materials and energies. Some fast MC codes also increase computational efficiency by taking advantage of various modern parallel processing technologies[26-29]. Recently, commercial vendors have also released fast MC codes in their TPSs (*e.g.*, Eclipse (Varian, Palo Alto, CA) and Raystation (Raysearch Lab, Stockholm, Sweden))[30,31]. These technological advances make fast MC calculation feasible for routine clinical use. However, the fast MC codes are confined to a few research institutions and limited to post-planning dose calculation. The MC based plan optimization[32,33], such as that in Raystation, would be essential to remedy dose calculation issues.

An in-house and open-source fast MC code, MCsquare[28,34], which is optimized and dedicated to pencil beam scanning (PBS) proton therapy simulations in voxelized geometries, such as a CT image, was employed. An open-source collaboration, OpenReggui, has integrated both MCsquare-based dose calculation and the planning tool MIROpt[33] to make fast MC-based post-planning evaluation and planning available to community hospitals, and to provide an ideal tool for collaboration among institutions or potentially for centralized auditing IROC/ NRG[35]. MCsquare was previously benchmarked with Geant4 simulations and validated by measurements for simple homogeneous and heterogeneous phantom geometries[28,36].

The purpose of this study was first to validate MCsquare for use in a clinical environment, and then to use it to calculate representative patient treatment plans for different clinical sites in order to explore the impact of ADC limitations on treatment plan quality. Schuemann *et al*[10] evaluated the effect of approximations in clinical analytical calculations in TPS on dosimetric indices for different sites of patients but limited the study to passive scattering proton therapy using TOPAS. Yepes *et al*[37] also reported a study for a large group of patients treated with intensity modulated proton therapy (IMPT) using their in-house fast track-repeating-based MC code but lacks analysis of the causes for the differences between Monte Carlo and TPS. In this study, we investigated the limitations of ADC with patients treated with single field uniform dose (SFUD) IMPT and explained the cause for the differences between open-source fast MCsquare, benchmarked with TOPAS, and ADC based on phantom measurements and patient case analysis as well.

This work is divided into the following three sections: 1) validation of MCsquare against both TOPAS and measurement for an anthropomorphic left lung phantom, and post-planning dose calculation comparison with TOPAS for selected PBS patient treatment plans; 2) extraction of clinically relevant dosimetric indices from dose distributions calculated by ADC and MCsquare on a large patient cohort covering five clinical sites, and comparison of the values of these indices between the two to assess the limitations of ADC; and 3) Specific patient examples analysis to better understand the physical causes for the differences between Monte Carlo dose calculation and ADC.

2. Methods

2.A Monte Carlo dose calculation

The Geant4-based TOPAS toolkit[16] has been extensively validated against measurements and widely used in all kinds of proton radiotherapy-related research[8,38-42]. It also provides advanced features for source modeling, complex geometry management, patient CT DICOM image processing with user defined material composition and density calibration curves, as well as multi-threaded operations. Here we used TOPAS (Version 2.0 built on Geant4.10.1p02) as the gold standard and benchmark tool for MCsquare. The default physics list containing the Geant4 modules (tsem-standard_opt3_WVI, g4h-phy_QGSP_BIC_HP, g4decay, g4ion-binarycascade, g4h-elastic_HP, and g4qstopping) in TOPAS was used in the simulation without modification.

The fast MC code, MCsquare, used in this study, was described in detail previously[28]. In contrast to a general purpose MC code, MCsquare is dedicated to proton PBS simulations in a voxelized geometry in order to improve calculation performance. Moreover, its implementation is optimized to exploit both task and data parallelisms of modern processors. MCsquare simulates the proton interactions with a class-II condensed history algorithm. The Multiple Coulomb scattering model proposed by Rossi and Greisen[43] was employed in MCsquare. Elastic and inelastic nuclear interactions are sampled from cross sections in the ICRU 63 report[44]. Heavy charged secondary particles are fully simulated by scaling proton stopping powers using the particle charge and mass, while electrons are locally absorbed and neutral particles are neglected. MCsquare is able to simulate 10^7 protons in less than a minute on a calculation server.

To commission both MC algorithms, the source model was determined by parameterizing the proton distribution at the exit of the PBS nozzle[21,45], which includes physics parameters such as the number of protons/MU and phase space parameters (beam size, angular divergence and energy spread). The major advantage of this method is that it does not require simulating the beam line or nozzle, significantly reducing computation time since there is no need to model and simulate particle transport through the nozzle. In order to recalculate complete patient treatment plans, an in-house tool based on Matlab was developed to convert the DICOM plan from a commercial TPS (Eclipse 13.7, Varian Medical Systems) into the phase space information for every single proton. Before importing patient DICOM files into TOPAS and MCsquare platforms, the CT values of structures such as the couch, patient bolus, and image artifacts were overwritten the same way as in the current clinical planning process. A method described by Schneider et al[46] to convert from HU to human tissues (including elemental composition, weights and densities) was also implemented. The dose in the patient was scored as dose-to-water[47] with the same resolution as the imported CT. Both MCsquare and TOPAS run the treatment plan simulations on a LINUX-based workstation with 72 cores (Intel Xeon E5-2699 v3 Processor).

2.B Anthropomorphic lung phantom and patient data

As MCsquare was previously benchmarked with Geant4 simulations and also validated by measurements for simple homogeneous and heterogeneous phantom geometries[28,36], here the focus is on the validation of MCsquare in realistic clinical situations. First, an anthropomorphic left lung phantom[48], made by the Imaging and Radiation Oncology Core (IROC) Houston Quality Assurance Center, was used to test the performance of different algorithms in a heterogeneous anatomy. We used the TPS to plan a treatment with two fields (left-right and anterior-posterior) using SFUD optimization method with a prescription dose to the PTV. The phantom irradiations were performed while the phantom was static (breath-hold approach). Within the left lung target insert, two thermoluminescent dosimeters (TLD, Thermo Fisher Scientific, Waltham, MA) and Gafchromic EBT3 films (Ashland, Dublin, OH) were used for absolute and planar dose measurements, respectively. The PBS plan, originally calculated with ADC, was recalculated with the commissioned TOPAS and MCsquare. The 3-dimensional dose distributions calculated with ADC and both MCs were submitted to IROC Houston to compare with film measurements over three cross-sectional views using a 2D gamma analysis[49] test with 7 %/5 mm criteria. To successfully pass the test, gamma passing rates must be higher than 85 %, the threshold defined by IROC Houston. These criteria are established based on the uncertainty of the dosimetry system and recommendations from the NCI cooperative groups[48].

In the second part of this study, 50 patients treated with PBS proton therapy in our clinic, covering five different sites: liver, pelvis, brain, head-and-neck, and lung (10 patients per site) were selected. All the patient's plans are optimized using conventional SFUD method following our clinical protocols. To account for random and systematic errors of patient setup, an additional margin is used to expand a CTV to a PTV. For lung and liver patients, the internal clinical target volume (iCTV) delineated by the union of CTVs on the corresponding eight-phase images of a 4DCT on average CT images was used instead. Each SFUD plan was then optimized to the planning target volume (PTV). The patient cohort is summarized in Table I, which indicates the range of prescription doses, target volumes, proton beam ranges, and modulation widths.

2.C Analysis process

From the patient cohort, the treatment plans of 20 patients (4 patients per site) were additionally recalculated using TOPAS and used as the reference to further validate the accuracy of MCsquare. Then all 50 patients' dose distributions predicted by ADC were compared to the recalculation results of MCsquare to assess the limitation of ADC in clinical situations. For both validation and assessment, 3D gamma index analysis (using 3 %/3 mm criteria), dosimetric indices, and tumor control probability (TCP) based on the dose-volume histograms (DVHs) were investigated.

After acquiring the 3D dose distributions, the following dosimetric indices and TCP values based on the DVHs of the target volume, specified either as the clinical target volume (CTV) or planning target volume (PTV), were used to compare the different algorithms:

- Mean target dose: the dose averaged over all voxels in the target.
- D95: the minimum dose that covers 95 % of the target volume.
- Dose heterogeneity index (HI, D5-D95): the difference between the minimum dose that covers 5 % and 95 % of the target volume.
- V95: the percentage of the target volume covered by a dose that is at least 90 % of the prescription.
- TCP: the tumor control probability calculated by an equivalent uniform dose (EUD)-based model[50] to quantify the clinical impact. TCP parameters were set according to the recommended values[10] (Table II).

The 3D gamma index distribution applying global normalization was also calculated by using a fast Euclidean distance transform method as described in Chen et al[51]. We used 3 %/3 mm criteria for both the target and the whole patient, and only voxels with a dose larger than 10 % of the prescribed dose were considered. 2%/2mm criteria was also used to compare MCsquare and TOPAS for a more restrictive validation.

Here a tissue heterogeneity index is proposed to facilitate the fast characterization of the level of longitudinal tissue heterogeneity for lung patients. In comparison to the heterogeneity index proposed by Soukup[52] to quantify the level of lateral heterogeneity, our heterogeneity index is defined as

$$\mathrm{H} = \frac{1}{N}\sum_i^N \int_{A_i}^{B_i} f(HU) = \begin{cases} 1, & HU < -500 \\ 0, & HU \geq -500 \end{cases} dz,$$

where N is the total number of voxels within the target volume, HU is the Hounsfield unit at each segmentation *dz* along the beam path from the patient surface, A_i, to the location of corresponding voxel, B_i. For the most part, H represents the average physical thickness of small density material, such as lung and air, which the proton beam traverses. H can be specified as the longitudinal tissue heterogeneity index.

3. Results

3.A Validation of MCsquare

Both Figure 1 and table III show that the MCsquare recalculation of the dose distribution in the anthropomorphic left lung phantom agrees well with both TOPAS simulation and measurements. Compared to MC calculations, ADC overestimated the output by 4 % and failed to agree with the IROC film measurement using the 7 %/5 mm gamma criteria. If MC calculations were used, the output would have agreed within 1 % of measurements. The gamma passing rate in the axial plane dramatically improved from 66 % for ADC to over 93 % for MC dose calculations, while the sagittal and coronal plane agreements improved from below 85 % for ADC, to over 98 % for MC calculations. From the 1D dose profile in the lower row, we can find that MC simulation agrees better with measurements than ADC. A shift (~5mm) between measurements and MC simulation can be found at the ramp up region in the anterior-posterior profile. This could be because of CT uncertainty and setup error during measurements. As the statistical uncertainty inherent in MC calculations might potentially bias the gamma passing rate of MC as opposed to ADC[53], the noise level of MC results was controlled to be below 1 % of the target dose—much smaller than the gamma criterion—to eliminate this concern.

The example presented in Figure 2 is for one of the lung patients, with high heterogeneity. Good agreement can be seen between the MCsquare- and TOPAS-calculated dose distributions. The result of ADC calculation is also added for comparison. The upper-row panels demonstrate a color wash distribution in the cross and coronal plane for the dose differences in TOPAS-MCsquare and ADC-MCsquare. The 1D dose profiles along the anterior-posterior, left-right and inferior-superior direction are shown in the bottom. A gamma index accumulative volume histogram is plotted in the bottom right panel. The histogram shows almost identical dose distributions between MCsquare and TOPAS, with 97.8% and 99.1% for 2%/2mm and 3%/3mm gamma passing rate respectively. Similar to the findings from the lung phantom analysis, figure 2 also shows that ADC consistently predicts higher dose and sharper penumbra than MC dose calculation. This is because the proton fluence along the central path of each pencil beam is predicted using the water-equivalent thickness along that beam path in ADC, and this will result in less lateral expansion of the spot than MC simulation where the divergent transportation of each particle in lung and air was simulated more accurately.

All the dosimetric indices mentioned in section 2.3 were determined for both TOPAS- and MCsquare-calculated dose distributions for the target volumes of the 20 patient plans selected for validation purposes; also computed was the passing rate for gamma index analysis performed between the two dose distributions. The corresponding relative differences with reference to TOPAS were obtained and are summarized in Table IV. The mean dose, D95, HI index, V95 calculated by MCsquare for all patients are within ±1.3 % of the indices calculated by TOPAS, while and TCP indices are within ±1.8%. The gamma analysis (3%/3 mm) passing rate for all voxels in the treatment field receiving dose above the 10 % threshold exceeds 99.0 % for every patient, with a median value of 99.9%. When only voxels within the target volume are considered, the passing rate has a median value of 100%. With a more restrictive criteria 2%/2mm, the gamma passing rate is slightly decreased with the minimum 95.28% and 97.26% for the target and patient, respectively. The median value is still larger than 99%. The differences between MCsquare and TOPAS can therefore be considered as not being significant with respect to the studied indices and scenarios.

3.B Assessment of ADC using MCsquare

Figure 3 depicts all dosimetric index differences and gamma index passing rates when comparing MCsquare and ADC for the 50 patients. Each data point in figure 3 corresponds to one patient plan, and boxplots were used to present the descriptive statistics. Each box plot has three lines: the bottom one represents the 25th percentile, the middle one corresponds to the median and the top one represents the 75th percentile.

Generally, the difference in the mean dose, D95, HI index, V95, and TCP between MCsquare and ADC increases as the heterogeneity increases from liver, to pelvis, to brain, to head-and-neck, and to lung. The maximum difference for the D95, HI index, V95 and TCP can be found for lung patients , while all the dose-related parameters are within -2.4%~1.4% for liver and pelvis patients. The largest TCP difference can be seen in lung (up to -10.1 %), while the TCP difference for liver, pelvis and brain is less than 2%.

The difference of the gamma index passing rate has a similar trend to the DVH-based indices, increasing as the heterogeneity increases, in general. 9 out of 10 liver, pelvis and brain patients have a gamma passing rate larger than 90% in both target and whole patient. The passing rate can be as low as 40 % for head-and-neck and lung patients. This can be explained by the results presented in the section 3.A, where ADC is seen to predict higher mean dose, while predicting a sharper penumbra compared to MCsquare. Lateral heterogeneity and range difference in the lung will also decrease the gamma index passing rate.

3.C Patient examples

The limited accuracy of ADC especially in lung patients has been widely reported[8,10,37,48], and similar results were found in this study too. Figure 4 presents a series of 4 lung patients with different tumor locations and with different degrees of heterogeneity in the paths of the beams used to treat them. The per cent dose difference (ADC-MCsquare) distribution and DVHs for the target and lung are plotted. The first patient, who had a pneumonectomy, had nearly no lung tissue in the treatment field because fluid filled the chest cavity, and hence there is excellent dose agreement except for some cold and hot spot due to range difference presumably caused by inaccurate simulation of ADC at the heterogeneous distal region. The DVHs for this patient calculated by ADC are essentially identical to those calculated by MCsquare. From then on, we can see the increase of lung tissue in the beam path and also the increase in discrepancy between MCsquare and ADC in the both 2D dose distribution and DVHs. The fourth patient presents the lung case with the largest mean dose difference within the target (-4.3 %). This patient was treated with beams passing through an anterior bolus. The extra air gap between the bolus and patient further increases the heterogeneity index of the geometry. By comparing the dose difference in the lung, we can find that ADC generally predicts lower dose in the periphery and conversely higher dose in the penumbra compared to MCsquare, leading to the tilt of the DVH curve of lung. This can be attributed to ADC's underestimation of the scattering effect at tissue interfaces. In reality more protons would be scattered by a larger distance from the target and into the lung, as modeled in MCsquare.

Figure 5 shows the gamma index passing rate of the treatment field of ADC plotted against the longitudinal tissue heterogeneity index (H). The data was fitted linearly and R^2 value was 0.88. It is thus demonstrated that there is a correlation between the degree of heterogeneity in the beam path and the dose computation inaccuracy.

Figure 6 shows the head-and-neck case and the brain case with the largest mean dose difference within the target of the 10 patients of each site (-3.4 % and -2.2 % respectively). For both cases, external devices (table-mounted variable pre-absorber for the head-and-neck case, patient-centered bolus for the brain case) were used to degrade the proton energies in order to treat these tumors located proximal to depths of 77 mm, which correspond to a proton range of 100 MeV in water, the minimum energy at the corresponding author's proton center. The dose discrepancy can be found in the penumbra region for both cases, which is caused by the inability of ADC to accurately describe the effects of MCS, especially when an air gap between the patient and the external devices exists. It is also worth noting that the dose discrepancy on the surface of the head-and-neck patient is larger than the interior. This is because the posterior-oblique neck fields are almost tangential to the patient surface, and ADC cannot properly model scattering at the air/tissue interface. MCsquare can obviously predict the amount of protons scattered out of the body more accurately than ADC. Contrary to the head-and-neck case, most protons will stop inside the patient for the brain case, though the mean dose of the target is overestimated and the penumbra issue still exists, albeit with smaller magnitude. The differences in range are presumably due to areas where the beam stops in either bone or air and cause the strip dose difference at the distal region of the fields.

4. Discussion

In this paper, we validated a fast and open-source MC code, MCsquare, using both measurements and TOPAS simulations in 20 patients. The analysis of dosimetric indices between the MCsquare and TOPAS yielded good agreement with less than 1.8% difference. The gamma index analysis for the 3%/3mm criteria resulted in a passing rate above 99% for all patients. However, the gamma index passing rate for the 2%/2mm criteria becomes slightly lower than that for the 3%/3mm criteria, but still larger than 95%. This could be because of the difference in nuclear model between TOPAS and MCsquare. Deviations up to 2% between MCsquare and Geant4 were reported for simple geometries[28]. Some slight differences in transverse dose profiles especially in the heterogeneous simulation are also reported in our previous study[28], which can be explained by the simplified multiple Coulomb scattering model. The statistical uncertainties in dose in each voxel may be another factor impacting the accuracy of the comparison.

After validation, MCsquare was applied to evaluate a 50 patient cohort covering the liver, brain, pelvis, head-and-neck, and lung disease sites to assess the deficiency of ADC and its impact on treatment plans. Schuemann et al [10] published results in a similar study for patients treated with passive scattering using TOPAS as a reference. Yepes *et al* reported the comparison results between MC dose calculation and TPS dose calculation for a large cohort of more than 500 patients[37] treated with IMPT. Our results showed that ADC can predict the dose distribution well for most patients with relatively homogeneous anatomy, such as liver and brain patients. Large differences can be found for lung and head-and-neck plans which demonstrates the shortcomings of ADC for dose calculation in heterogeneity. Our results agree with both Yepes' and Schuemann's findings. All the treatment plans reported in our study are optimized with SFUD method, which is one limitation of our study. Multifield optimization (MFO) IMPT plans have been implemented in to clinical practice to explore the greatest benefit from proton therapy, although interfield gradients unique to MFO IMPT come with a high risk of dose degradation. The interfield gradients in the penumbra and distal fall-off position of MFO IMPT plans could potentially worsen the performance of ADC in heterogeneity as expected. Robust MFO optimization technique which is increasingly available in commercial TPS can result in more reproducible dose distributions to account for setup errors and range calibration uncertainties compared to conventional MFO plans.

For those head-and-neck and lung patients, the ADC consistently predicts a higher mean dose to the target and sharper penumbra compare to MC dose calculation. Besides, dose difference, both cold and hot spots, can be also found at the distal fall-off region due to range differences. These dose discrepancy between ADC and MC algorithm are mainly caused by inaccurate modeling of MCS in heterogeneous geometry in the ADC. Soukup concentrates on the analysis of impact of the lateral heterogeneity in geometries on dose accuracy and proposed a heterogeneity index to quantify the level of lateral heterogeneity. The limitation of their index is that it doesn't consider the inaccurate modeling of protons' scattering in the low-density lung/air following interacting with chest wall, which domains in lung patients. Based on a simple idea that the more lung/air thickness in the beam path will lead to larger difference between ADC and MC calculation, we proposed an approximate tissue heterogeneity index for the lung patients to quickly quantify the level of longitudinal heterogeneity for lung cases. The high degree of correlation between this heterogeneity index and the overall gamma passing rate between ADC- and MCsquare-calculated dose distributions highlights the impact that tissue/air interfaces along the beam path have on plan calculation accuracy. As our longitudinal heterogeneity index only considers the heterogeneity along the beam path, a combination of both longitudinal and Soukup's lateral tissue heterogeneity index could be a more appropriate index to represent the level of the heterogeneity of patients. A potential application of this index is that it can quickly quantify the level of heterogeneity, presumably predict how much we can benefit from using MC dose calculation and then decide whether MC algorithm is necessary or not with respect to different time consumption between ADC and MC algorithm.

Besides of the anatomy heterogeneity of patient itself, external devices such as couch, range modulation devices (bolus, range shifter, and aperture, etc.) could also increase the heterogeneity of dose calculation and thus requires more accurate fast MC calculations. For example, in the author's clinic, a patient-centered bolus and a table-mounted pre-absorber must be used in order to deliver PBS treatment plans using the IBA treatment delivery system whose lowest proton energy is 100 MeV (range of 77 mm). A U-shaped head bolus is used to treat brain tumors (as shown in section 3.C patient examples) with better efficiency and plan quality[54] than a range shifter (RS), which is far away from the patient in the dedicated nozzle on our fixed beam line. The advantage of these range-degradation devices is that they can be put as close as possible to patients to mitigate the air gap, providing smaller spot size and higher plan quality. Although the air gap can be potentially limited by a movable RS implementation, there still could be large air gaps between the RS and the treatment couch for posterior oblique beams required for head-and-neck patients, which would degrade the plan quality. One other mitigation strategy, suggested by Titt et al[55], used variable pre-absorbers. The Paul Scherrer Institute (PSI) has implemented such an approach using multiple 4 mm RS plates. Using such an approach can dramatically sharpen the penumbra for superficial tumors as they can be closer to the patients with minimal air gaps. However, such implementations would require commercial TPS vendors to release accurate dose calculation engines, such as fast MC codes. Otherwise, the current implementation of these external devices drawn as structures on the CT and calculated by the ADC in the TPS would increase the heterogeneity of the geometry and further increase the inaccuracy of ADC potentially.

Analytical algorithms are computationally efficient and commonly used in TPSs for dose calculation and treatment plan optimization. More accurate MC-based algorithms including fast MC algorithms are mainly used for post-planning dose verification. MC-based optimization is essential to overcome the impact of the limited accuracy of ADC on the treatment plan quality. Figure 7 presents the lung case, treated with two posterior oblique fields, which displayed the largest D95 difference between ADC and MCsquare shown in figure 3. For this case, we generated a new plan using the MCsquare-based optimizer, MIROpt[33]. From the DVH in the figure 7, it can be observed that the dose recalculated by MCsquare reflects significant degradation of D95 by 6.8 % and of the HI index by 6.0 % compared to what the ADC would indicate. In this case, treatment plans optimized based on MC beamlets provide better evaluation DVH than plans based on analytical beamlets.

The calculation time for MCsquare is just a small fraction of the corresponding time for TOPAS simulation, when using the same initial number of particles. In general, MCsquare is able to simulate 10 million protons in less than 1 minute, while TOPAS requires approximately 1 hour for the same number of protons simulated on the same workstation. In this study, 400 million initial protons were simulated per patient, leading to approximately 1 % of statistical uncertainty in the target region for the dose computed with the same resolution as CT images (typically 1 x 1 x 2.5 mm^3). In real clinical applications, the statistical uncertainties of each voxel should be calculated during simulation, like using batch method[56], to determine whether number of simulated histories is large enough to satisfy the uncertainty requirements. The number of particles to be simulated, and therefore the computation time, can be further decreased if using a coarser dose resolution (typically 2.5 x 2.5 x 2.5 mm^3) instead of the resolution of CT images. TOPAS's parallel simulation capability was limited by memory size and this issue was resolved by more efficient use of memory in MCsquare. The high speed of MCsquare limits the time consumption of treatment planning using MIROpt to 40 mins for this lung case. Future works will aim at conducting investigation of MIROpt's application on more patients and other treatment sites such as head-and-neck.

In addition to dose calculation, MCsquare is also able to compute LET distributions. Figure 8 illustrates the dose and LET distributions computed by MCsquare for one of the brain cases. The method described by Cortés-Giraldo and Carabe[57] is implemented in MCsquare to compute the dose-averaged LET (LETd). Due to the large angle scattering and secondary particles, the LETd distribution spread far away from the beam path. For this reason, high LETd values may be located in the very low dose regions, making the interpretation of the distribution very complex. Therefore, the dose-weighted LETd distribution, resulting from the voxel-wise multiplication of the dose and LETd distributon, is also presented in figure 8(c), from which we can find a significant part of the OAR is covered by high LET values because both proton beams are directed toward the brain stem. This illustration shows the importance of LET verification and Monte Carlo calculation during the treatment plan evaluation.

Implementation of MCsquare for dose calculation does not require specific demanding hardware. MCsquare is compatible with all current standard computers and operating systems. A plugin was implemented in the OpenReggui application in order to provide a graphical interface for MCsquare and to convert the DICOM files into the appropriate format. This plugin is released as open source with OpenReggui. Users are also encouraged to develop their own scripts to interface MCsquare with their TPS. As with every dose engine, a commissioning procedure is required to generate a beam model for MCsquare. We are currently developing a tool to automatically extract the beam parameters from the commissioning measurement typically performed during the TPS commissioning. We are testing this tool for various proton therapy equipment, including IBA, Varian, and Hitachi machines. It will also be released as open source in the future.

5. Conclusions

In this paper, the accuracy of a fast MC code, MCsquare, was validated by comparing its results with IROC lung phantom measurements and the results of TOPAS. The accuracy and time efficiency of MCsquare facilitated the assessment of the impact of ADC on the treatment quality of 50 patients covering various sites. Agreement within 2 % of dosimetric indices was found for most liver and pelvis patients. Large dose differences for highly heterogeneous head-and-neck and lung cases can result in large TCP differences, up to 10 % for lung and up to 6 % for head-and-neck. Given the differences found in these analyses, validated fast MC dose calculations are recommended for routine treatment plan quality assurance, at least for the challenging sites like head-and-neck and lung, and fast MC dose calculation based optimization techniques are highly needed to further explore the potential advantage of proton therapy. The fully open source setting of MCsquare enables great flexibility and adaptability in a manner potentially suited for institution collaboration and centralized auditing.

Conflict of interest

The authors have no conflicts to disclose.

References:

1. Hong L, Goitein M, Bucciolini M, et al. A pencil beam algorithm for proton dose calculations. *Phys Med Biol.* 1996;41(8):1305-1330.
2. Schaffner B, Pedroni E, Lomax A. Dose calculation models for proton treatment planning using a dynamic beam delivery system: an attempt to include density heterogeneity effects in the analytical dose calculation. *Phys Med Biol.* 1999;44(1):27-41.
3. Szymanowski H, Oelfke U. Two-dimensional pencil beam scaling: an improved proton dose algorithm for heterogeneous media. *Phys Med Biol.* 2002;47(18):3313-3330.
4. Ciangaru G, Polf JC, Bues M, Smith AR. Benchmarking analytical calculations of proton doses in heterogeneous matter. *Med Phys.* 2005;32(12):3511-3523.
5. Soukup M, Fippel M, Alber M. A pencil beam algorithm for intensity modulated proton therapy derived from Monte Carlo simulations. *Phys Med Biol.* 2005;50(21):5089-5104.
6. Ulmer W, Schaffner B. Foundation of an analytical proton beamlet model for inclusion in a general proton dose calculation system. *Radiation Physics and Chemistry.* 2011;80(3):378-389.
7. Yao W, Merchant TE, Farr JB. A simplified analytical random walk model for proton dose calculation. *Phys Med Biol.* 2016;61(20):7412-7426.
8. Grassberger C, Daartz J, Dowdell S, Ruggieri T, Sharp G, Paganetti H. Quantification of proton dose calculation accuracy in the lung. *Int J Radiat Oncol Biol Phys.* 2014;89(2):424-430.

9. Paganetti H. Range uncertainties in proton therapy and the role of Monte Carlo simulations. *Phys Med Biol.* 2012;57(11):99-117.
10. Schuemann J, Giantsoudi D, Grassberger C, Moteabbed M, Min CH, Paganetti H. Assessing the Clinical Impact of Approximations in Analytical Dose Calculations for Proton Therapy. *International Journal of Radiation Oncology Biology Physics.* 2015;92(5):1157-1164.
11. Fippel M, Soukup M. A Monte Carlo dose calculation algorithm for proton therapy. *Med Phys.* 2004;31(8):2263-2273.
12. Zhu XR, Poenisch F, Lii M, et al. Commissioning dose computation models for spot scanning proton beams in water for a commercially available treatment planning system. *Med Phys.* 2013;40(4):041723.
13. Agostinelli S, Allison J, Amako K, et al. Geant4—a simulation toolkit. *Nuclear Instruments and Methods in Physics Research Section A: Accelerators, Spectrometers, Detectors and Associated Equipment.* 2003;506(3):250-303.
14. Waters LS, Hendricks J, McKinney G. MCNPX Los Alamos National Laboratory, Los Alamos, NM. 2005.
15. Battistoni G, Cerutti F, Fassò A, et al. The FLUKA code: description and benchmarking. *Hadronic Shower Simulation Workshop (American Institute of Physics).* 2007:31-49.
16. Perl J, Shin J, Schümann J, Faddegon B, Paganetti H. TOPAS: An innovative proton Monte Carlo platform for research and clinical applications. *Med Phys.* 2012;39(11):6818-6837.
17. Jan S, Santin G, Strul D, et al. GATE: a simulation toolkit for PET and SPECT. *Phys Med Biol.* 2004;49(19):4543-4561.
18. Sawakuchi GO, Titt U, Mirkovic D, Mohan R. Density heterogeneities and the influence of multiple Coulomb and nuclear scatterings on the Bragg peak distal edge of proton therapy beams. *Phys Med Biol.* 2008;53(17):4605-4619.
19. Sawakuchi GO, Titt U, Mirkovic D, et al. Monte Carlo investigation of the low-dose envelope from scanned proton pencil beams. *Phys Med Biol.* 2010;55(3):711-721.
20. Schuemann J, Dowdell S, Grassberger C, Min CH, Paganetti H. Site-specific range uncertainties caused by dose calculation algorithms for proton therapy. *Phys Med Biol.* 2014;59(15):4007-4031.
21. Grevillot L, Bertrand D, Dessy F, Freud N, Sarrut D. A Monte Carlo pencil beam scanning model for proton treatment plan simulation using GATE/GEANT4. *Phys Med Biol.* 2011;56(16):5203-5219.
22. Tourovsky A, Lomax AJ, Schneider U, Pedroni E. Monte Carlo dose calculations for spot scanned proton therapy. *Phys Med Biol.* 2005;50(5):971-981.
23. Kohno R, Takada Y, Sakae T, et al. Experimental evaluation of validity of simplified Monte Carlo method in proton dose calculations. *Phys Med Biol.* 2003;48(10):1277-1288.
24. Fippel M. Fast Monte Carlo dose calculation for photon beams based on the VMC electron algorithm. *Med Phys.* 1999;26(8):1466-1475.
25. Li JS, Shahine B, Fourkal E, Ma CM. A particle track-repeating algorithm for proton beam dose calculation. *Phys Med Biol.* 2005;50(5):1001-1010.
26. Wan Chan Tseung H, Ma J, Beltran C. A fast GPU-based Monte Carlo simulation of proton transport with detailed modeling of nonelastic interactions. *Med Phys.* 2015;42(6):2967-2978.
27. Jia X, Schumann J, Paganetti H, Jiang SB. GPU-based fast Monte Carlo dose calculation for proton therapy. *Phys Med Biol.* 2012;57(23):7783-7797.
28. Souris K, Lee JA, Sterpin E. Fast multipurpose Monte Carlo simulation for proton therapy using multi- and many-core CPU architectures. *Med Phys.* 2016;43(4):1700-1712.
29. Yepes PP, Mirkovic D, Taddei PJ. A GPU implementation of a track-repeating algorithm for proton radiotherapy dose calculations. *Phys Med Biol.* 2010;55(23):7107-7120.

30. Lin L, Huang S, Kang M, et al. A benchmarking method to evaluate the accuracy of a commercial proton monte carlo pencil beam scanning treatment planning system. *J Appl Clin Med Phys.* 2017;18(2):44-49.
31. Saini J, Maes D, Egan A, et al. Dosimetric evaluation of a commercial proton spot scanning Monte-Carlo dose algorithm: comparisons against measurements and simulations. *Phys Med Biol.* 2017;62(19):7659-7681.
32. Ma J, Beltran C, Seum Wan Chan Tseung H, Herman MG. A GPU-accelerated and Monte Carlo-based intensity modulated proton therapy optimization system. *Med Phys.* 2014;41(12):121707.
33. Barragán Montero AM, Souris K, Sanchez-Parcerisa D, Sterpin E, Lee JA. Performance of a hybrid Monte Carlo-Pencil Beam dose algorithm for proton therapy inverse planning. *Med Phys.* 2018;45(2):846-862.
34. http://www.openmcsquare.org/.
35. Giaddui T, Chen W, Yu J, et al. Establishing the feasibility of the dosimetric compliance criteria of RTOG 1308: phase III randomized trial comparing overall survival after photon versus proton radiochemotherapy for inoperable stage II-IIIB NSCLC. *Radiation Oncology.* 2016;11(1):66.
36. Sorriaux J, Testa M, Paganetti H, et al. Experimental assessment of proton dose calculation accuracy in inhomogeneous media. *Physica Medica: European Journal of Medical Physics.*38:10-15.
37. Yepes P, Adair A, Grosshans D, et al. Comparison of Monte Carlo and analytical dose computations for intensity modulated proton therapy. *Phys Med Biol.* 2018;63(4):045003.
38. Testa M, Schümann J, Lu HM, et al. Experimental validation of the TOPAS Monte Carlo system for passive scattering proton therapy. *Med Phys.* 2013;40(12):121719-n/a.
39. Grassberger C, Lomax A, Paganetti H. Characterizing a proton beam scanning system for Monte Carlo dose calculation in patients. *Phys Med Biol.* 2015;60(2):633-645.
40. Paganetti H, Jiang H, Lee SY, Kooy HM. Accurate Monte Carlo simulations for nozzle design, commissioning and quality assurance for a proton radiation therapy facility. *Med Phys.* 2004;31(7):2107-2118.
41. Paganetti H, Jiang H, Parodi K, Slopsema R, Engelsman M. Clinical implementation of full Monte Carlo dose calculation in proton beam therapy. *Phys Med Biol.* 2008;53(17):4825-4853.
42. Lin L, Kang M, Solberg TD, Ainsley CG, McDonough JE. Experimentally validated pencil beam scanning source model in TOPAS. *Phys Med Biol.* 2014;59(22):6859-6873.
43. Rossi B, Greisen K. Cosmic-Ray Theory. *REVIEWS OF MODERN PHYSICS.* 1941;13(4):240-309.
44. ICRU. Nuclear data for neutron and proton radiotherapy and for radiation protection. *ICRU Report 63.* 2000.
45. Huang S, Kang M, Souris K, et al. Validation and clinical implementation of an accurate Monte Carlo code for pencil beam scanning proton therapy. *J Appl Clin Med Phys.* 2018;0(0).
46. Schneider W, Bortfeld T, Schlegel W. Correction of CT artifacts and its influence on Monte Carlo dose calculations. *Med Phys.* 2007;34(6):2119-2132.
47. Paganetti H. Dose to water versus dose to medium in proton beam therapy. *Phys Med Biol.* 2009;54(14):4399-4421.
48. Taylor PA, Kry SF, Followill DS. Pencil Beam Algorithms Are Unsuitable for Proton Dose Calculations in Lung. *International Journal of Radiation Oncology • Biology • Physics.* 2017;99(3):750-756.
49. Low DA, Harms WB, Mutic S, Purdy JA. A technique for the quantitative evaluation of dose distributions. *Med Phys.* 1998;25(5):656-661.
50. Gay HA, Niemierko A. A free program for calculating EUD-based NTCP and TCP in external beam radiotherapy. *Physica Medica: European Journal of Medical Physics.*23(3):115-125.

51. Chen M, Lu W, Chen Q, Ruchala K, Olivera G. Efficient gamma index calculation using fast Euclidean distance transform. *Phys Med Biol.* 2009;54(7):2037.
52. Soukup M, Alber M. Influence of dose engine accuracy on the optimum dose distribution in intensity-modulated proton therapy treatment plans. *Phys Med Biol.* 2007;52(3):725-740.
53. Huang JY, Pulliam KB, McKenzie EM, Followill DS, Kry SF. Effects of spatial resolution and noise on gamma analysis for IMRT QA. *J Appl Clin Med Phys.* 2014;15(4):93-104.
54. Both S, Shen J, Kirk M, et al. Development and Clinical Implementation of a Universal Bolus to Maintain Spot Size During Delivery of Base of Skull Pencil Beam Scanning Proton Therapy. *International Journal of Radiation Oncology • Biology • Physics.*90(1):79-84.
55. Titt U, Mirkovic D, Sawakuchi GO, et al. Adjustment of the lateral and longitudinal size of scanned proton beam spots using a pre-absorber to optimize penumbrae and delivery efficiency. *Phys Med Biol.* 2010;55(23):7097-7106.
56. Sempau J, Sánchez-Reyes A, Salvat F, Tahar HOb, Jiang SB, Fernández-Varea JM. Monte Carlo simulation of electron beams from an accelerator head using PENELOPE. *Phys Med Biol.* 2001;46(4):1163.
57. Cortés-Giraldo MA, Carabe A. A critical study of different Monte Carlo scoring methods of dose average linear-energy-transfer maps calculated in voxelized geometries irradiated with clinical proton beams. *Phys Med Biol.* 2015;60(7):2645.

Figures and caption list

Figure 1: Axial and sagittal view of the IROC proton lung phantom with field arrangement indicated. A: Anterior; L: Left; P: Posterior; R: Right; Sup: Superior; Inf: Inferior, with dose profile through the center of the planning target volume (PTV) in the left-right, posterior-anterior, and inferior-superior directions. Film measurements are shown in black, the ADC algorithm result in blue, TOPAS in red and MCsquare in cyan. The vertical dashed line represents the PTV which corresponds to the yellow contour on the CT images.

Figure 2: Comparisons of ADC and MCsquare, and TOPAS and MCsquare for a lung treatment plan: dose difference (a)(b) (ADC-MCsquare) , (c)(d) (TOPAS-MCsquare) , line profile along (e) anterio-posterior, (f) left-right and (g) superior-inferior direction, (h) accumulative volume histogram of their gamma index. The visible structure (red contour on the CT images) is iCTV.

Figure 3: Summarized analysis of the dosimetric impact of ADC on treatment plan quality by comparison with MCsquare: (left) box plot of percentage difference (MCsquare-ADC) for 5 sites (liver, pelvis, brain, head-and-neck, and lung) for 5 dosimetric parameters of the target (mean dose, D95, D95-D5, V95, and TCP); (right) box plot of Gamma-index passing rate with 3 %/3 mm criteria for all patients including voxels in the target volume alone, and including all voxels in the patient with dose above the 10 % threshold. On each box, the central mark indicates the median, and the bottom and top edges of the box indicate the 25th and 75th percentiles, respectively.

Figure 4: Dose comparison between MCsquare (dashed line) and ADC (solid line) for four consecutive representative lung cases with different heterogeneity: upper row: the dose difference (ADC-MCsquare); lower row: corresponding DVHs for the internal clinical target volume (iCTV) and the selected organ (total lung and ipsilateral lung).

Figure 5: 3D gamma passing rate with 3 %/3 mm criteria of the treatment field between MCsquare and ADC for 10 lung patients versus the longitudinal tissue heterogeneity index (H).

Figure 6: Dose comparison between MCsquare (dashed line) and ADC (solid line) for one selected head-and-neck and brain case with the largest mean dose difference within the target of the 10 patients of each site: upper row: the dose difference (ADC-MCsquare); lower row: corresponding of DVHs for the clinical target volume (CTV: red contour) and the selected organ.

Figure 7: A new treatment plan using MCsquare-based optimization: (left): 2D dose distribution on a selected axial plane; (right) DVH comparison between the original plan in the TPS calculated by ADC and MCsquare, and the new plan generated by the MCsquare-based optimizer MIROpt.

Figure 8. The dose and LET distributions calculated by MCsquare for a brain case: (a) dose distribution in Gy; (b) dose-averaged LET (LETd) distribution in keV/µm; (c) dose-weighted LET distribution (voxel-wise multiplication of the dose and LET distributions) on a selected coronal plane. The red and yellow contours represent the brain stem and the target respectively.

Tables

Table I: Summary of the treatment characteristics of the patient cohort

Treatment site	Number of patients	Range of target volumes (cc)	Range of prescription doses (Gy(RBE))	Range of beam ranges (mm)	Range of modulation widths (mm)
Liver	10	10-1133	45.0–67.5	134-289	44-201
Pelvis	10	42-543	45.0-70.2	226-316	85-241
Brain	10	6-299	40.0-66.6	100-280	36-202
Head and neck	10	17-177	54.0-66.6	127-284	54-197
Lung	10	46-230	50.0-66.6	176-273	64-148

Table II: Parameters used in the TCP calculations for liver, brain, pelvis (prostate/rectum/anal), head-and-neck and lung tumors.

Tumor sites	**α/β (Gy)**	**a**	**v_{50}**	**D_{50} (Gy)**
Liver	10	-10	1.20	53.00
Brain	10	-10	0.75	27.04
Prostate	2	-10	2.25	75.5
Rectum/anal	10	-10	1.66	46.97
Head-and-neck	10	-10	2.25	51.77
Lung	10	-10	3.52	74.50

ǂ α/β = alpha-beta ratio; a is a unitless EUD model parameter that is specific to tumor of interest; D_{50} and v_{50} represent the dose needed for 50% tumor control and the slope of the response curve at that point, respectively.

Table III: The gamma passing rate of ADC in Eclipse (TPS) and independent MC dose calculations (TOPAS and MCsquare) in comparison with film measurement embedded in the IROC anthropomorphic left lung phantom, and dose ratio of TLD measurements to ADC/TOPAS/MCsquare. 7 %/5 mm criteria were used in gamma comparison.

	Film Plane (Gamma Index)			TLD	
	Axial	Coronal	Sagittal	Superior	Inferior
ADC	66%	82%	83%	0.96	0.96
TOPAS	93%	98%	99%	0.99	0.99
MCsquare	96%	99%	98%	0.99	0.99

Table IV: Summary of the difference in dosimetric indices and of gamma index analysis between MCsquare and TOPAS using 3 %/3 mm and 2%/2mm criteria.

	Dosimetric indices (MCsquare-TOPAS)					Gamma index (3%/3mm)		Gamma index (2%/2mm)	
	D_{mean}(%)	D95(%)	HI(%)	V95(%)	TCP(%)	Target	Patient	Target	Patient
Median	-0.17	-0.15	-0.45	0	-0.04	100	99.89	99.08	99.28
Min~Max	-1.20~0.42	-1.00~0.39	-1.26~0.54	-0.85~0.90	-1.80~0.34	99.30~100	99.02~100	95.28~100	97.26~99.84

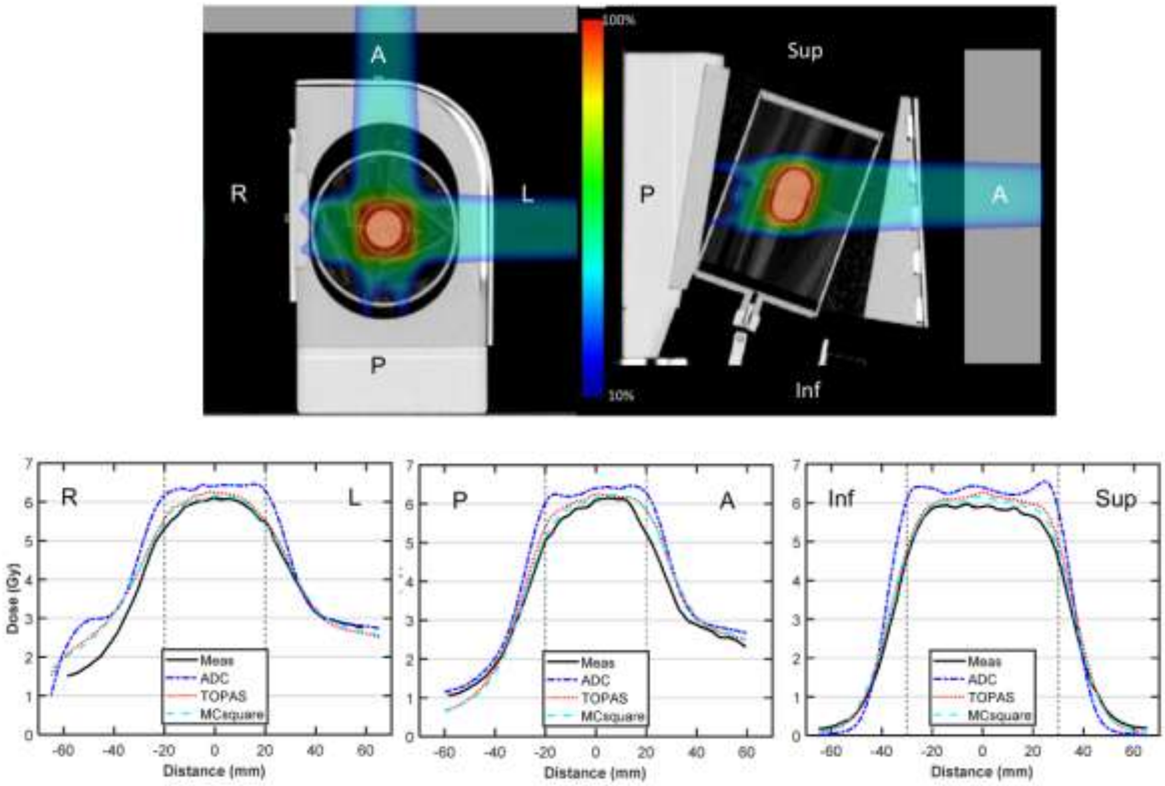

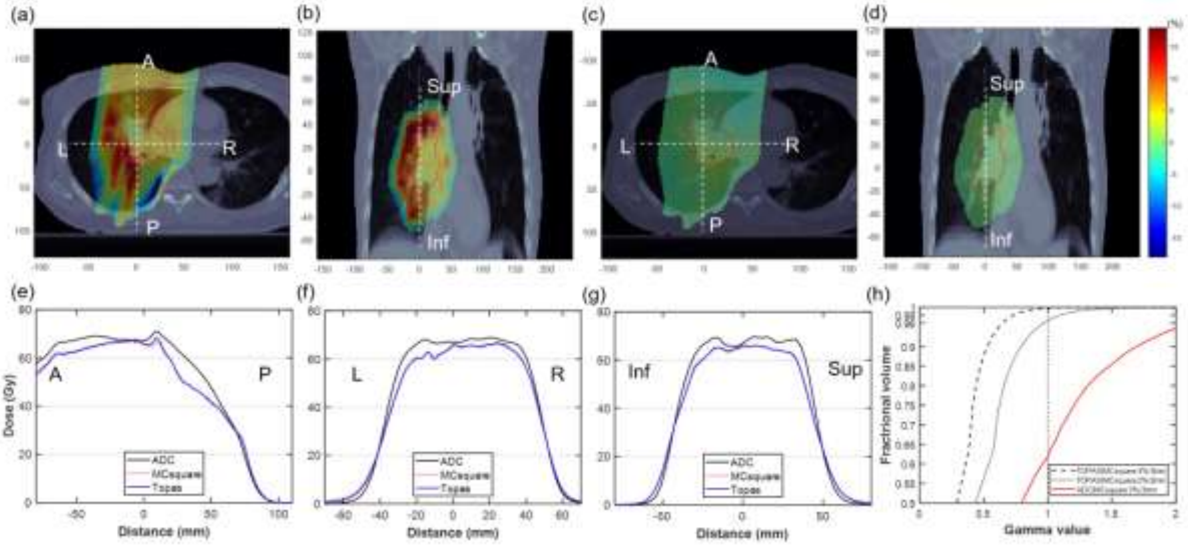
(a)
(b)
(c)
(d)
(e)
(f)
(g)
(h)
A
P
L
R
Sup
Inf
ADC
MCsquare
Topas
Dose (Gy)
Distance (mm)
Fractional volume
Gamma value

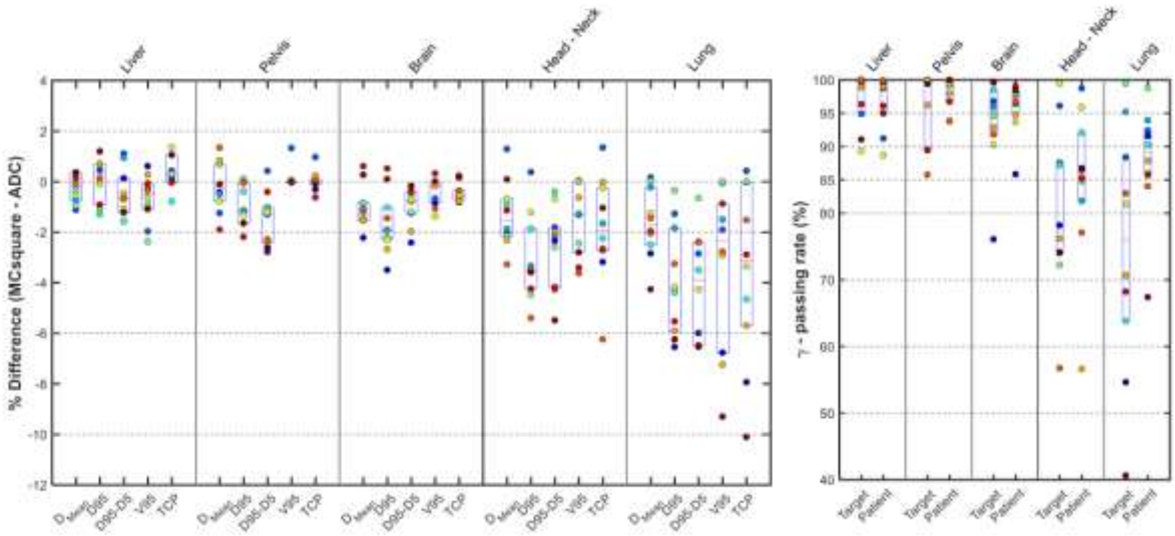
Liver
Pelvis
Brain
Head - Neck
Lung
% Difference (MCsquare - ADC)
γ - passing rate (%)
D95
D95-D5
V95
TCP
Target
Patient

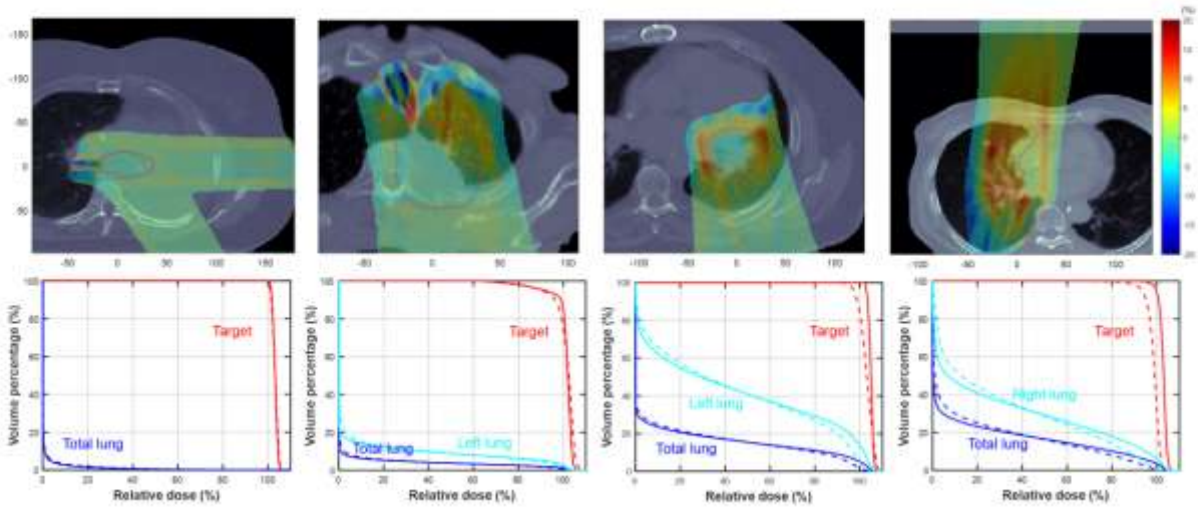
Target
Total lung
Left lung
Right lung
Volume percentage (%)
Relative dose (%)

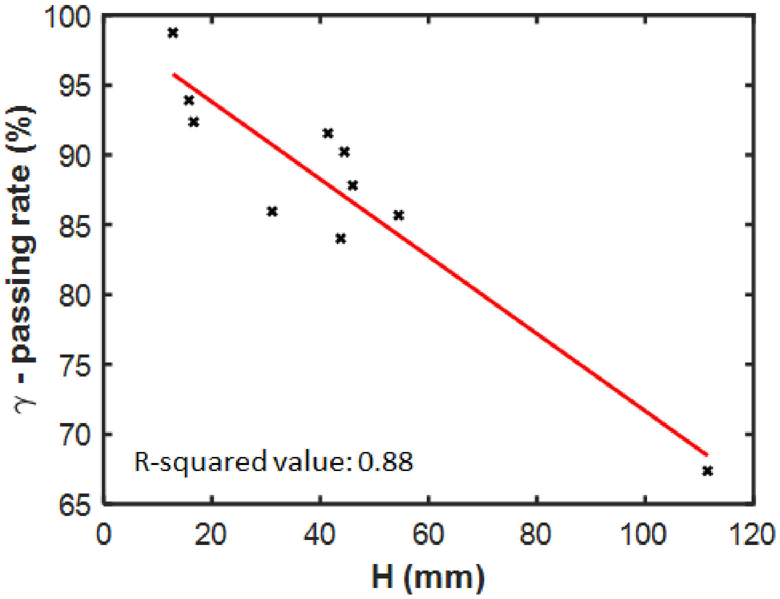
100
95
90
85
80
75
70
65
γ - passing rate (%)
R-squared value: 0.88
0
20
40
60
80
100
120
H (mm)

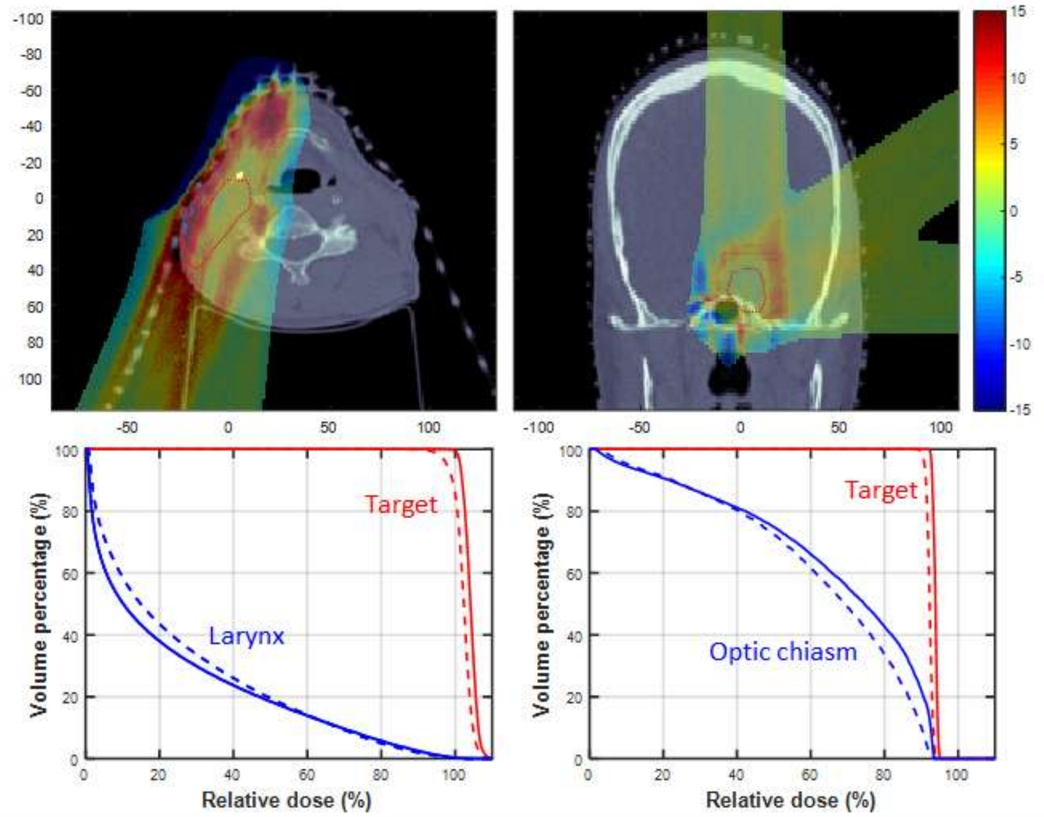

Target
Larynx
Volume percentage (%)
Relative dose (%)
Target
Optic chiasm
Volume percentage (%)
Relative dose (%)

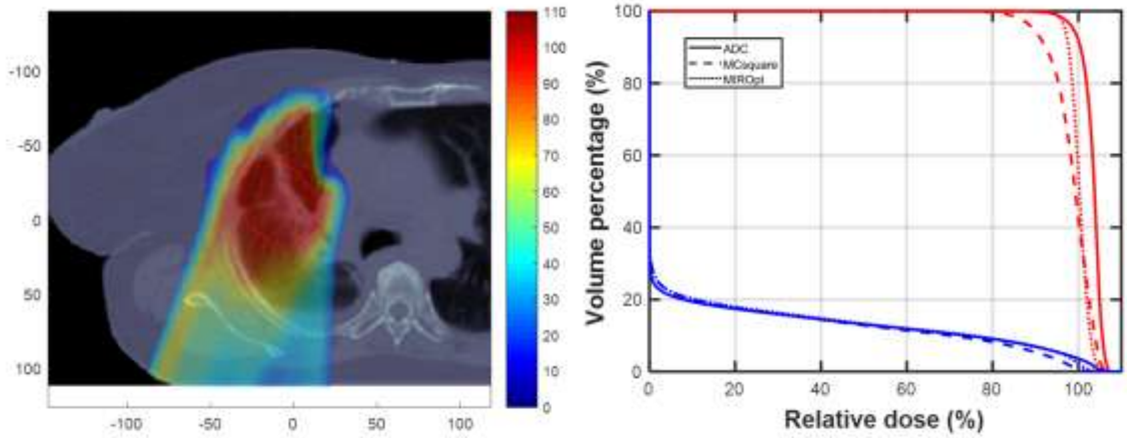
ADC
MCsquare
MIROpt
Volume percentage (%)
Relative dose (%)

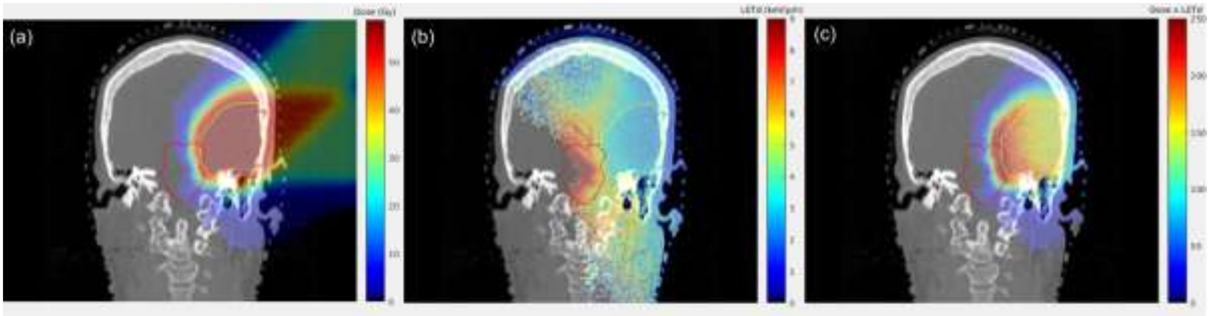
(a)
(b)
(c)